

An LES-Like Multiscale Multiphase Flow Model Based on Break-up and Coalescence Phenomena

M. M. Noroozi, R. Maddahian[†], M. H. Ramezani and M. R. Ansari

Faculty of Mechanical Engineering, Tarbiat Modares University, Tehran, Iran

[†]Corresponding Author Email: maddahian@modares.ac.ir

(Received September 19, 2021; accepted January 20, 2022)

ABSTRACT

The multiscale multiphase flow contains both small-scale (dispersed phase) and large-scale (continuous phase) structures. Standard interface-averaging multiphase models are appropriate for the simulation of flows including small-scale structures. Standard interface-resolving multiphase models are commonly used for the simulation of flow regimes containing large-scale structures. The accurate simulation of different regimes has a crucial role to investigate the physics of multiphase flows. To cover the inability of standard models to simulate multiscale multiphase flows, various generalized hybrid models have been developed. The present research aims to present an LES-like approach to identify the large-scale structures by comparing the equivalent diameter of structures and the averaging length scale. The main difference between the presented model and the models available in the literature is the independency of the model to the thresholds of the local volume fraction to recognize the flow regime. The switching criterion is set based on the cell size and the physical phenomena including the break-up and coalescence mechanisms. To assess the capabilities of the presented multiscale model, four different benchmark cases including the bubble column, the impinging jet, the dam break, and the Rayleigh-Taylor instability are investigated. The physical behavior of the flow is considered as a reference and compared with numerical results. It is demonstrated that the present multifluid model is capable to capture the physical characteristics of both dispersed and segregated flow regimes, and it is a forward step to develop a generalized multiscale hybrid multiphase model.

Keywords: Multiphase flow; Computational multiphase fluid dynamics; Transient flow regime; Hybrid model; Multiscale model.

NOMENCLATURE

d	equivalent diameter	a	volume fraction
F	force	δ	interface disturbance
g	gravity acceleration	ρ	density
M	inter-phase momentum transfer	μ	dynamic viscosity
p	pressure	ν	kinematic viscosity
t	time		
\vec{u}	velocity vector		

1. INTRODUCTION

Multiphase flows exist in different fields of industry (Brennen 2005; Kolev 2005; Schwarzkopf *et al.* 2011; Shu *et al.* 2019; Yeoh and Tu 2009). One of the main challenges in the multiphase flow modeling is the co-existence of various flow regimes in a shared domain. Due to the complicated flow field and the turbulence-induced effects, the continuous phase with large-scale structures may be broken up into dispersed phase with small-scale structures or

vice versa, and different interfacial structures are formed (Rusche 2002). The simultaneous existence of different flow structures makes the numerical simulation quite challenging. Therefore, a unique generalized numerical approach that could be used in different flow regimes is necessary. During the last two decades, the lack of a comprehensive model that can capture the flow regime transitions or handle the multiscale flow regimes has been quite noticeable (Hänsch *et al.* 2012; Marschall 2011; Mathur *et al.* 2019; Wardle and Weller 2013).

The preliminary idea of multiscale models was the simultaneous use of the multifluid models and the surface tracking/capturing models. [Cerne *et al.* \(2001\)](#) presented a model by coupling the two-fluid and the Volume Of Fluid (VOF) models. A switching criterion was proposed based on the gradient of volume fraction across the cell to recognize the computational cells being solved either by the VOF or two-fluid approaches. The main complexity of their approach was the necessity of solving various equations in a shared computational domain. The multifluid model framework has more generality than the interface capturing methods. [Denèfle *et al.* \(2015\)](#) employed the three-phase concept which included the continuous liquid, small bubble gas, and large bubble gas phases. The large-scale bubbles were modelled using the interface capturing approach. Also, the mass transfer terms between the continuous and dispersed gas phases were ignored. A similar method was employed by [Yan and Che \(2010\)](#). The VOF and two-fluid approaches were adopted to model large and small length scale structures, respectively. A method called “volume fraction redistribution” was utilized for the interfacial interaction terms in cells occupied by all phases. Only the coalescence of small-scale gas phase to large-scale gas phase was considered in this model. The most important limitation of the model was the failure to guarantee the conservation of liquid and small-scale gas in the parts of the domain where all three phases simultaneously exist. The weakness and complexity of the mentioned approaches have led researchers to focus their efforts on developing a general multifluid approach.

[Höhne and Vallée \(2010\)](#) presented the Algebraic Interfacial Area Density (AIAD) model. The main feature of the model was its ability to model the momentum transfer terms by linking them to the flow morphology. The AIAD model was able to make difference between bubbles, droplets, and the free surface by using the volume fraction value. To distinguish the dispersed and the segregated zones, the blending functions were introduced. The interfacial forces corresponding to the flow regime were also handled using the blending functions. [Hänsch *et al.* \(2012\)](#) extended the AIAD model and presented a novel concept called the GENeralised TwO-Phase flow (GENTOP). The inhomogeneous Multiple Size Group (iMUSIG) approach was employed to model the mass transfer terms between the small-scale and large-scale gas phases. The main problem with the GENTOP model was the utilization of artificial sharpening force on the interface without any physical support. [Coste *et al.* \(2013\)](#) followed a similar approach. To ensure the segregated-like treatment of the large interface structures present within the domain, a Large Interface Model (LIM) was coupled with a standard two-fluid model. The large-scale structures identification process was done by means of the gradient of a sharpened volume fraction field. The interfacial transfer closure models were computed over a three-cell stencil across the interface. This model was developed with the purpose of stratified liquid and gas flow regimes simulation. The surface tension effect was not contributed in the calculations. By coupling the

Eulerian multifluid framework with the interface sharpening method, a new hybrid methodology was developed by [Wardle and Weller \(2013\)](#). The model was developed in the context of the Open-source CFD software OpenFOAM. [Shonibare and Wardle \(2015\)](#) extended Wardle’s hybrid multiphase solver. The new solver was improved by adding a new interface sharpening algorithm. The interface sharpening criterion was based on the comparison of the local mean diameter and the local mesh size. The dispersed phase diameter was also predicted by utilizing the reduced PBM and an algebraic model based on the critical Weber number. A hybrid Eulerian model called the Large-Scale Interface (LSI) model was developed by [Gada *et al.* \(2017\)](#). The model distinguished between the different morphologies based on blending functions. The blending functions have similar characteristics to the weighting function used in the AIAD model. The interface identification approach of [Coste *et al.* \(2013\)](#) was used in the LSI model to capture the interfacial cells. Also, in order to discretize the volume fraction field, an Adaptive Interface Scheme (ADIS) was utilized. The ADIS discretization method is a combination of the High-Resolution Interface Capturing (HRIC) scheme and the Total Variation Diminishing (TVD) scheme. Later, [Mathur *et al.* \(2019\)](#) developed the Hybrid Dispersed-Large Interface Solver (HD-LIS) model in the context of the OpenFOAM code. A flow regime map was employed to make difference between the dispersed and segregated flow regimes. They used the TVD discretization schemes and the semi-implicit temporal discretization approach to keep the solution bounded and stable. Also, to control the numerical diffusion problem on the interface, a numerical compression was utilized, and the turbulence damping model was employed to imitate the wall-like behaviour of the interface. Recently, [Meller *et al.* \(2020\)](#) established a GENTOP-like framework in OpenFOAM based on the multiphase EulerFOAM solver. They derived a morphology adaptive modeling framework that is capable to handle the coexistence of the unresolved interfacial structured and resolved interfacial structures in the computational domain with the same set of equations. The capability of model to handle the multiscale flow was evaluated by two test cases; a 2D gas bubble rising in a liquid field, and a 2D stagnant stratification of water and oil ([Meller *et al.* \(2020\)](#)).

The literature review shows that the preliminary hybrid model was numerically complex due to the existence of different sets of governing equations in the same domain. Recent hybrid methods employ the multifluid concept including an interface sharpening algorithm to resolve the interface between phases. [Hänsch *et al.* \(2012\)](#) proposed a generalized Eulerian-based model by coupling CFD and PBM. The GENTOP model has been still developing by adding new effective features and extensions to make the simulations much more realistic and reliable ([Höhne *et al.* 2019; Höhne *et al.* 2017; Montoya *et al.* 2015; Montoya *et al.* 2014](#)). All the models reviewed in the literature have some imperfections, like using unphysical numerical models and

formulations (Hänsch *et al.* 2012), ignoring the polydispersity of dispersed phase structures (Cerne *et al.* 2001; Denèfle *et al.* 2015; Gada *et al.* 2017; Mathur *et al.* 2019; Wardle and Weller 2013), lack of a consistent model for four field approach (complete consideration of both droplets and bubbles) (Denèfle *et al.* 2015; Gada *et al.* 2017; Hänsch *et al.* 2012), and ignoring the effects of turbulent issues (e.g. bubble induced turbulence effects) (Denèfle *et al.* 2015; Gada *et al.* 2017; Hänsch *et al.* 2012; Liao *et al.* 2020; Mathur *et al.* 2019; Meller *et al.* 2020; Parekh and Rzehak 2018; Shonibare and Wardle 2015). Therefore, multiscale issues have not yet been noticed extensively within the unique modelling framework and many sections need improvement to make the models much more generalized.

The present study aims to develop a Computational Fluid Dynamic-Population Balance Model (CFD-PBM) based on the Eulerian-Eulerian multifluid model. The changes of bubble size distribution due to the physical phenomena like bubble breakage and coalescence are captured using the iMUSIG model. These physical phenomena are connected to the modelling approach. The size groups' adjustment is set in a way to have a physical background. The LES-like behaviour of the model leads to use the grid as a resolving filter. In this concept the grid is used as a switching criterion between the interfacial scale resolving and the interfacial scale averaging approaches and vice versa. The interfacial closure models for the large-scale and the small-scale structures are blended by a flow regime map concept. Furthermore, the physical-based selection of numerical schemes and mass transfer models, makes the solver capable to capture the underlying flow physics for dispersed, segregated and multiscale flow regimes.

2. GOVERNING EQUATIONS AND MATHEMATICAL MODELS

In the present research, the multi-fluid model reported by Rusche (2002) is adopted. The continuity and the momentum equations are presented in Eq. (1) and (2), respectively.

$$\frac{\partial(\rho_\varphi \alpha_\varphi)}{\partial t} + \nabla \cdot (\rho_\varphi \alpha_\varphi \vec{u}_\varphi) + F_{IC,\varphi} = 0 \quad (1)$$

$$\frac{\partial(\rho_\varphi \alpha_\varphi \vec{u}_\varphi)}{\partial t} + \nabla \cdot (\rho_\varphi \alpha_\varphi \vec{u}_\varphi \vec{u}_\varphi) = -\alpha_\varphi \nabla p + \nabla \cdot (\mu_\varphi \alpha_\varphi \nabla \vec{u}_\varphi) + \rho_\varphi \alpha_\varphi g + M_\varphi \quad (2)$$

The subscript φ denotes the arbitrary phase (i.e. the dispersed or segregated phases), α is the volume fraction, ρ , μ and p are the density, dynamic viscosity, and pressure, respectively. g is the acceleration due to gravity, and M_φ denotes the averaged interphase momentum transfer term. $F_{IC,\varphi}$ also represents the interface compression scheme. The interface compression term is calculated by the numerical methodology presented by Weller (Wardle and Weller 2013; Weller 2008).

2.1 LES-like Multiscale Physical Model

A novel approach is used to distinguish between different structures in a flow field. As a multiscale multifluid framework, three different phases are considered, including the primary phase, the large scale and small-scale secondary phases. Both secondary phases are known as the Eulerian phases but different approaches are used to model the momentum interaction terms. In the hybrid models, the interfacial scale averaging and the interfacial scale resolving closure frameworks are used for dispersed and segregated flow regimes, respectively. The coupling process of these modeling approaches leads to complex and unphysical distinguishing methodologies between different morphologies. As shown in Fig. 1, the partially interfacial scale resolving closure framework (Marschall 2011) is employed in the present work for large-scale structures. The large-scale interface is demonstrated as a transition region by assuming the partially interfacial scale resolving closure framework. In the present model, the small-scale and large-scale secondary phases are treated as a penetrating and a partially penetrating Continuum, respectively.

Analogously to the LES model idea, the averaging length scale is used as a filter to detect the large-scale structures. As shown in Fig. 2, if the mean diameter size of the secondary phase is larger than the cell size, the partially interfacial scale resolving closure framework is used and the interface between phases is resolved. Otherwise, the interfacial scale averaging closure framework is utilized. Many different physical phenomena can be considered in numerical simulations. Considering the physical concepts results the realistic flow behaviour. Krepper *et al.* (2008) utilized the iMUSIG model to handle the polydispersity in their simulations. The iMUSIG makes their model capable to capture the lift force inversion phenomena and the flow development along a vertical pipe. Hänsch *et al.* (2012) introduced the complete coalescence mass transfer mechanism to reflect the physical phenomenon of coalescence on the interface in the GENTOP concept. All these steps are in line to develop the physical models. In the present work, the mass transfer between large and small scales is considered employing the coalescence and breakup of particles. The mass transfer mechanisms due to the coalescence and breakup phenomena are handled using Luo (1995) and Luo and Svendsen's (1996) models, respectively. The size groups characteristics are set according to the grid size in a way that the mass transfer between the phases occurs based on the averaging length scale. So the closure modeling framework is switched along with the coalescence or breakup phenomenon. This concept is described graphically in Fig. 2. If the small-scale structures coalesce together and make a large-scale structure, both mass transfer, and closure modeling framework substitution, occur simultaneously.

2.2 Interphase Momentum Transfer

Considering the multi-fluid concept, the interfacial momentum transfers (M_φ) should be modeled. The interphase momentum transfer term contains the

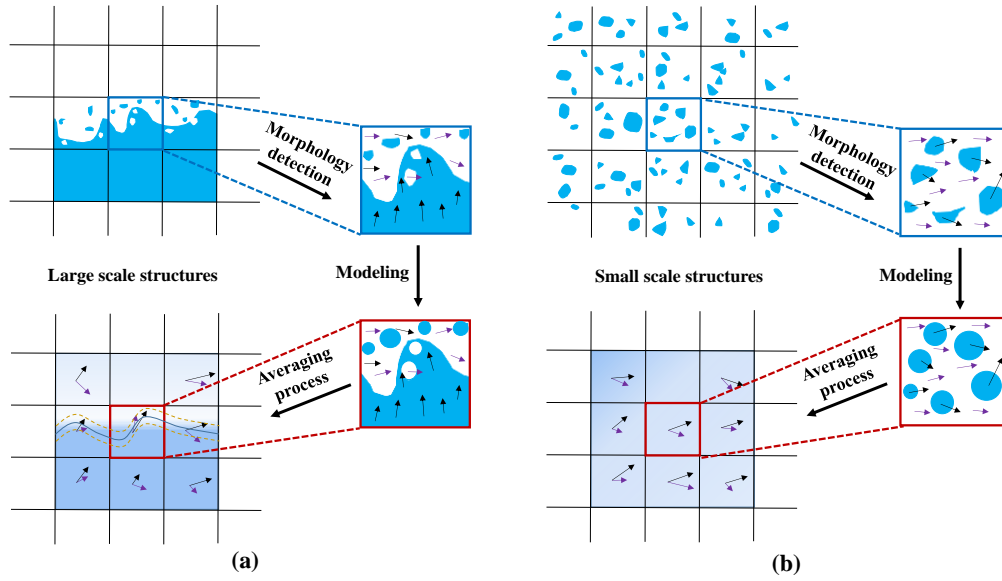


Fig. 1. Graphical representation of the interfacial scale closure frameworks for a multifluid model (Marschall 2011), (a) large-scale structures, (b) small-scale structures.

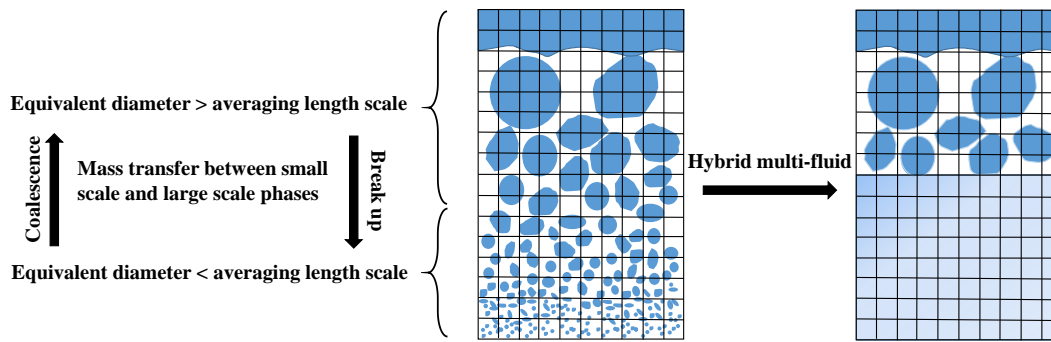


Fig. 2. Graphical representation of coupling hybrid multifluid concept with population balance model.

following interfacial closure models:

$$M_\phi = F_d + F_l + F_{vm} + F_{td} + F_{wl} + F_{st} \quad (3)$$

where F_d , F_l , F_{vm} , F_{td} , F_{wl} , and F_{st} represent the instantaneous drag, lift, virtual mass, turbulent dispersion, wall lubrication, and surface tension forces, respectively. The interfacial models are described in Table 1.

The interphase momentum transfers depend on the flow regime. Segregated and dispersed closures are blended as a function of the local void fraction. Therefore, the concept of blending functions is employed. Blending functions are the weight functions used to implement the interfacial forces according to the flow regimes. The inter-phase forces can be estimated for different flow regimes using Eq. (4).

$$F_T = F_D \phi_D + F_S \phi_S + F_B \phi_B \quad (4)$$

where F_T , F_D , F_S , and F_B are the total, droplet flow, segregated flow, and bubbly flow forces, respectively. ϕ_D , ϕ_S , and ϕ_B are also the droplet,

segregated and bubbly blending functions. A hyperbolic Blending function is used to implement the interfacial forces (Greenshields 2019).

2.3 Interface Compression

In order to sharpen the interphase between resolved scales, the interface compression algorithm should be employed in the concept of Eulerian framework. A numerical methodology presented by Weller (Wardle and Weller 2013; Weller 2008) is used in the present work to control the numerical diffusion on the interface. The interface compression term on the left-hand side of Eq. (1) is written as:

$$F_{IC,\phi} = \nabla \cdot (\phi_{IC} \vec{u}_c \alpha_\phi (1 - \alpha_\phi)) \quad (5)$$

where, \vec{u}_c is the compression velocity which is employed for interface sharpening. The compression velocity should be applied in the segregated flow regimes. ϕ_{IC} is a weighting function equals to one at the vicinity of the interface. The weighting function gradually tends to zero far from the interface (Wardle and Weller 2013).

Table 1 Interphase force models

Interphase force	Model	Formulation
Dispersed flow drag	Ishii <i>et al.</i> (Ishii and Zuber 1979)	$F_{dragDispersed} = -\frac{3C_D}{4} \frac{\rho_c \alpha_d}{d_d} \vec{u}_d - \vec{u}_c (\vec{u}_d - \vec{u}_c)$ $C_D = \max(C_{D,sphere}, \min(C_{D,ellipse}, C_{D,cap}))$ $C_{D,sphere} = \frac{24}{Re_p} (1 + 0.1 Re_p^{0.75})$ $C_{D,ellipse} = \frac{2}{3} \sqrt{Eo}$ $C_{D,cap} = \frac{8}{3}$ $Eo = \frac{\Delta \rho g d_d^2}{\gamma}$
Segregated flow drag	Marschall (Marschall 2011)	$F_{dragSegregated} = (m Re_I + n \pi_\mu) \frac{ \nabla \alpha_\phi }{\delta} \frac{\bar{\mu}_\phi \bar{\mu}_\phi}{\bar{\mu}_\phi + \bar{\mu}_\phi} (\vec{u}_\phi - \vec{u}_\phi)$ $Re_I = \frac{\rho_m \delta \vec{u}_\phi - \vec{u}_\phi }{\alpha_\phi \alpha_\phi (\bar{\mu}_\phi \bar{\mu}_\phi / (\bar{\mu}_\phi + \bar{\mu}_\phi))}$ $\pi_\mu = \frac{\alpha_\phi \alpha_\phi (\bar{\mu}_\phi \bar{\mu}_\phi / (\alpha_\phi \bar{\mu}_\phi + \alpha_\phi \bar{\mu}_\phi))}{\bar{\mu}_\phi \bar{\mu}_\phi / (\bar{\mu}_\phi + \bar{\mu}_\phi)}$
Lift	Tomiyama (Tomiyama <i>et al.</i> 2002)	$F_{lift} = -C_c \rho_c \alpha_d (\vec{u}_d - \vec{u}_c) \times (\nabla \times \vec{u}_c)$ $C_L = \begin{cases} \min[0.288 \tanh(0.121 Re_b), f(Eo_d)] & Eo_d < 4 \\ f(Eo_d) & 4 < Eo_d < 10 \\ -0.27 & Eo_d > 10 \end{cases}$ $f(Eo_d) = 0.0015 Eo_d^3 - 0.0159 Eo_d^2 - 0.0204 Eo_d + 0.474$
Virtual mass	Constant value	$F_{vm} = -C_{vm} \alpha_d \rho_c \left(\frac{D_d \vec{u}_d}{Dt} - \frac{D_c \vec{u}_c}{Dt} \right)$ $C_{vm} = 0.5$
Turbulent dispersion	Burns (Burns <i>et al.</i> 2004)	$F_{td} = -C_{TD} K_{c,d} \frac{D_c}{\sigma_{td}} \left(\frac{\nabla \alpha_d}{\alpha_d} - \frac{\nabla \alpha_c}{\alpha_c} \right)$ $D_c = \frac{\mu_{t,c}}{\rho_c}$ $C_{TD} = 1$ $\sigma_{td} = 0.9$
Wall lubrication	Tomiyama (Tomiyama <i>et al.</i> 1998)	$F_{wl} = C_{wl} \rho_c \alpha_d \vec{u}_c - \vec{u}_d ^2 \vec{n}_w$ $C_{wl} = C_w \frac{d_b}{2} \left(\frac{1}{y_w^2} - \frac{1}{(D - y_w)^2} \right)$ $C_w = \begin{cases} 0.47 & Eo < 1 \\ e^{-0.933 Eo + 0.179} & 1 \leq Eo \leq 5 \\ 0.00599 Eo - 0.0187 & 5 \leq Eo \leq 33 \\ 0.179 & 33 \leq Eo \end{cases}$
Surface tension	Brackbill (Brackbill <i>et al.</i> 1992)	$F_{st} = \sigma_{st} \kappa \nabla \alpha$ $\kappa = -\nabla \cdot \left(\frac{\nabla \alpha}{ \nabla \alpha } \right)$

2.4 Turbulence Modeling

In The Reynolds stresses which are created by the averaging of the governing equations should be modeled using the appropriate turbulence model. The *k-ω* Shear Stress Transport (SST) is employed

in the present work (Menter 1994). In the SST model, a special blending function with the capability of switching between the *k-ε* and *k-ω* models in the different regions of flow is employed. Using the empirical wall function to bridge the low Reynolds region to the far-away turbulent flow region is avoided in the *k-ω* SST model and thus provides a

better prediction of the fluid velocity near the wall region (Cheung *et al.* 2007). This is perfectly in line with the purpose of the present research and enables a more realistic capturing of the flow features. The governing equations of the $k-\omega$ SST model could be found in (Liao *et al.* 2020; Menter 1994).

3. SOLUTION METHODOLOGY

The solver is developed in the context of the Open-source Computational Fluid Dynamics (CFD) toolbox, OpenFOAM version 8. In the present research, the multiphaseEulerFoam solver is used. This multiphase solver contains all the pre-requisite models to develop the multiscale multifluid model. To minimize the numerical diffusion effect, the high-resolution TVD (Total Variation Diminishing) scheme is utilized for the advection terms. Also, to discretize the volume fraction and the advection terms, the Van Leer (Van Leer 1979) the limited linear (Greenshields 2019) schemes are employed, respectively. For the pressure equation, the Geometric Algebraic Multi-Grid (GAMG) iterative method is employed. The PIMPLE algorithm (Greenshields 2019) handles the linkage between pressure and velocity fields. Also, the Multi-dimensional Limiter for Explicit Solution (MULES) (Greenshields 2019) limiter is used in the main solver to maintain the phase volume fraction fields bounded and stable.

To select the optimum grid size, a primary assessment simulation is performed for each test case. The primary simulation gives an overview of flow physics and bubbles size distribution. The grid size could be selected according to the bubbles' size distribution and the filtered interfacial structures (Cerne *et al.* 2001; Marschall 2011; Marschall and Hinrichsen 2013). By reducing the averaging length scale, more interfacial structures are resolved. Furthermore, the purpose of simulation and the computational resources are also effective in the grid size selection. Enabling proper handling of the resolved interfaces on a coarser resolution is an ongoing research topic (Marschall 2011; Marschall and Hinrichsen 2013; Hänsch *et al.* 2012). The grid is uniform for all test cases and all ranges of bubble size are simulated with the same grid size. Due to the physical characteristics of the flow and the flow structures, the cell sizes are not the same in different test cases.

4. RESULTS AND DISCUSSION

Four different Test Cases (TC) are considered to validate the developed multiphase solver. TC1 is a bubble column which is considered to demonstrate the formation of large-scale structures. The mass transfer due to the coalescence of small-scale structures is evaluated in TC1. The impinging liquid jet with gas entrainment (TC2) is taken into account to assess the mass transfer mechanism due to the breakup from the continuous large-scale structures to the polydispersed small-scale structures. One of the main features of the presented solver is the interfaces sharpening methodology that is used as an extension to the multi-fluid solver. The dam break benchmark

(TC3) which is a well-known test case for interface-resolving models is employed to evaluate the sharpening methodology. Finally, the capabilities of the developed model in terms of capturing the physical behavior of the transitional multiphase flow, particularly transition between the dispersed and the continuous interfacial structures, are evaluated in TC4 through the simulation of the Rayleigh-Taylor instability. TC4 is one of the most suitable test cases to evaluate the hybrid transitional multiphase model (Chandrasekhar 2013; S'trubelj and Tiselj 2008).

4.1 Bubble Column

The dispersed air is injected from the bottom of a water column. The coalescence and breakup phenomena may occur when the injected bubbles rise due to buoyancy effect. A 2D uniform grid with 4000 elements of 5 mm is used for the simulation of flow field in TC1. Two air phases, small-scale, and large-scale are defined including 8 size groups. The diameter of air bubbles varies from 1 mm to 9 mm. The largest size group of the small-scale air has an equivalent diameter size equal to the grid size. For all phases, the no-slip condition is used on the side walls. The inlet mass flow of dispersed air containing the smallest bubble size group is applied at the bottom of the computational domain. A continuous large-scale air is considered above water level. On the top patch of the domain, an opening boundary condition is applied. The considered boundary conditions and the geometry of domain are shown in Fig. 3.

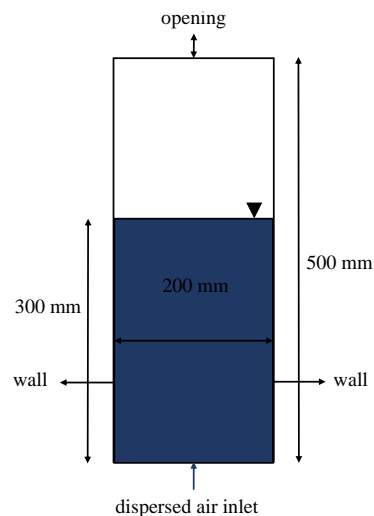


Fig. 3. Computational domain and boundary conditions for the bubble column (TC1).

As a result of the coalescence phenomenon, large-scale air structures may form from the dispersed small-scale air phase. By using the interface sharpening method, it is possible to capture the transition from small-scale to large-scale structures. The volume fraction of small and large scales air is demonstrated in Fig. 4. Small-scale bubbles start to rise from the bottom of the column after entering the domain. Due to the coalescence phenomena, the small bubbles move upward and coalesce to form

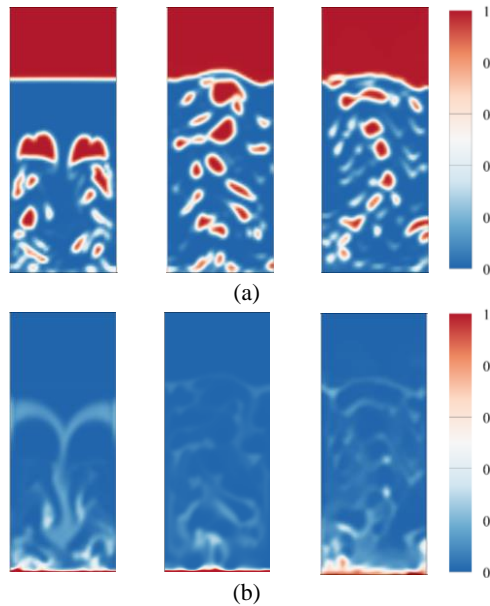


Fig. 4. Volume fraction field for small-scale and large-scale air phase in a bubble column, (a) large-scale air, (b) small-scale air.

larger bubbles. During the movement of bubbles, if the coalescence phenomenon creates bubbles larger than the grid size, the mass transfer occurs from the small-scale to the large-scale air phase. The interface between large-scale air phase and water is captured using the interface sharpening method. As the mass transfer between the continuous large-scale air and the dispersed small-scale air starts, the continuous air volume fraction value arises. Figures 4(a) and 4(b) show the volume fraction of air phases. The typical spherical and ellipsoidal large-scale bubble shapes can be captured during the simulation. The blending function is also employed to implement the appropriate momentum transport between phases. In the bubble column test case, it is common to form a large-scale bubble chain in the middle of the domain. As shown in Fig. 4(a), the present simulations also capture the bubble chain due to the coalescence processes and mass transfers from the small-scale air phase to large-scale air phase.

4.2 Impinging Liquid Jet

TC2 is an impinging liquid jet with gas entrainment which is configured according to experimental measurements of Danciu *et al.* (Danciu *et al.* 2010; Melzer 2018). The computational domain and boundary conditions are shown in Fig. 5. The jet velocity (v_j), length (L_j), and diameter (d_j) are equal to 1.7 m/s, 100 mm, and 16 mm, respectively. A uniform 2D structured grid with a cell size of 4 mm is employed for numerical simulations. The no-slip boundary condition is considered on the column wall. To keep the water level constant, the mass flow rate equal to the jet mass flow rate is set on the bottom of the domain. Two air phases including the small and large scales are defined consisting of 10 bubble size groups ranging from $d_{min}=1$ mm to $d_{max}=5$ mm. The air structure larger than the cell size is represented by the continuous large-scale air

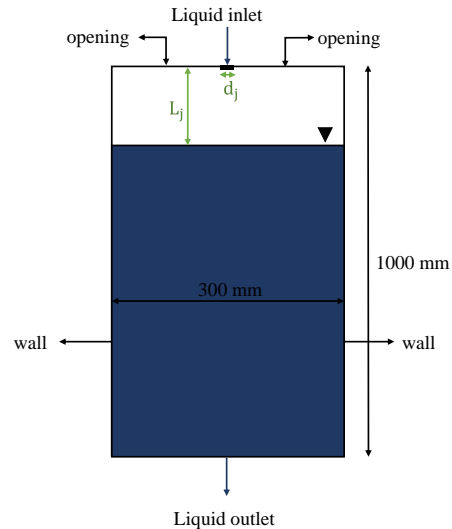


Fig. 5. Computational domain and boundary conditions for the impinging jet (TC2).

phase. The air and water properties are considered at temperature of 25 °C.

The time variations of the dispersed and continuous air during the jet impingement is shown in Fig. 6. Two large-scale air bubbles are created by impinging the water jet ($t = 0.033$ s). The maximum turbulence and flow instabilities occur on the air-water interface which result the breakup of continuous air. Over time, the volume fraction of large-scale continuous air decreases due to the breakup and mass transfer from the large scale to the small scale air. The simulation results show that the main entrainment process begins right after the initial air cavity pinches off which in accordance with experimental measurements (Zhu *et al.* 2000). As shown in Fig. 6, two large-scale air structures are separated from the free surface continuous air and starts to breakup ($t = 0.04$ s). The breakup process continues until the complete transfer of large-scale air to the small one. When the jet-induced momentum at the bottom of the column dissipates, the movement direction changes, and the small-scale structures rise upwards and return to the free surface ($t > 0.27$ s). The numerical results are also compared with experimental measurements in Fig. 6. A good qualitative analogy can be seen between the experimental data and numerical results. The downward motion of large-scale air and the upward bubbles' motion in the numerical simulations are completely in agreement with previous works (Qu *et al.* 2011; Hänsch *et al.* 2011).

The jet penetration depth at different times were extracted from the experimental pictures (Melzer 2018), via the image processing algorithm. Figure 7 shows the numerical penetration depth at different times compared with the experimental data (Melzer 2018). The numerical simulation results of TC2 showed good agreement with the experimental data. The maximum difference between numerical results and experimental data occurs at 0.071 s. At that time, the bubbles start to breakup, and the solution

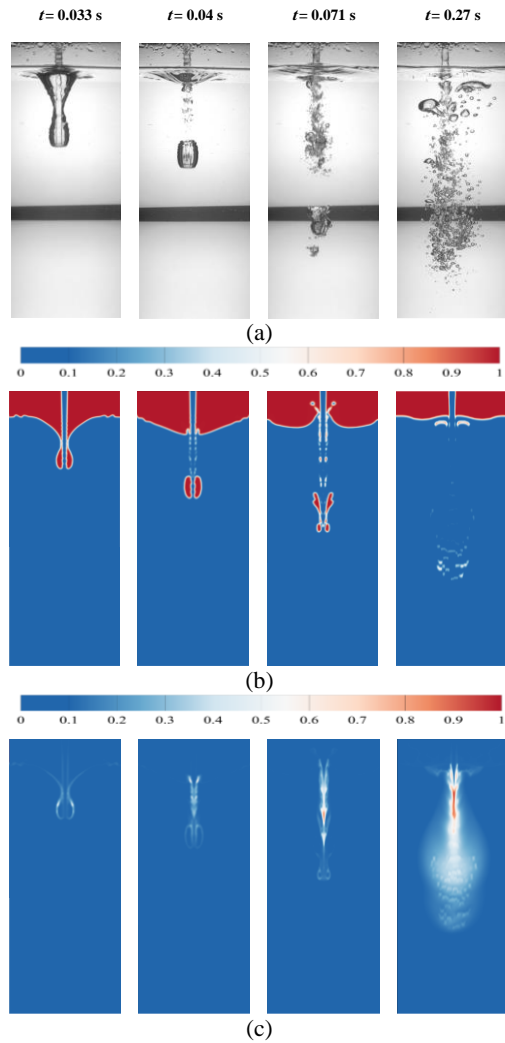


Fig. 6. Comparison of experimental data (Melzer 2018) and the time variations of small and large scale air volume fractions for the impinging water jet case, (a) experimental data (Melzer 2018), (b) large-scale air, (c) small-scale air.

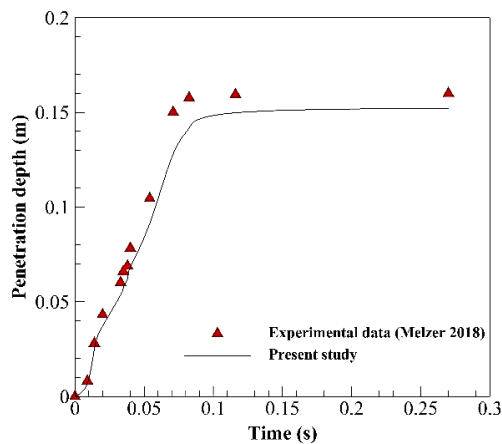


Fig. 7. Calculated penetration depth of jet compared with the experimental data (Melzer 2018).

approach changes from the partially averaging to the averaging closure framework.

To investigate the effectiveness and capability of switching criterion between resolving and non-resolving interfaces, the mass transfer rate between small and large scales air is logged during simulations and shown in Fig. 8. Before jet impingement on the water surface, the mass transfer is negligible. The mass transfer starts by the jet impingement and intensifies when the two large bubbles starts to breakup ($t = 0.05$ s). The maximum mass transfer is seen at $t = 0.1$ s, when the trapped bubbles are completely broken up to small bubbles. The variations of mass transfer show the appropriate working of multiscale model.

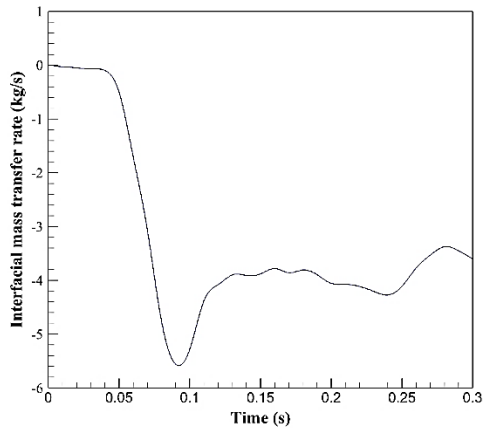


Fig. 8. Mass transfer rate over time between the large and small-scales air in TC2.

4.3 Dam Break

The dam break with an obstacle is considered as TC3. As shown in Fig. 8, the computational domain is adjusted according to Koshizuka's experiments (Koshizuka 1995; Ubbink 1997). A uniform 2D grid with 21244 computational cells is considered for numerical simulations. The cell size is 4 mm.

The simulations are performed using the multifluid framework. Two air phases with 8 bubble size groups are defined ranging from 1 mm to 10 mm. The maximum small-scale phase diameter is 4 mm which is equal to filtering size. The fluids' properties are calculated at temperature of 25 °C. The initial and boundary conditions are shown in Fig. 9. The no-slip condition is adjusted on the walls. An inletOutlet opening boundary condition is also utilized on the top boundary with the relative pressure of 0 Pa.

The flow features during the dam break at the six different times are compared to experimental data (Koshizuka 1995; Ubbink 1997) and shown in Fig. 10. By opening the gate, the water column accelerates due to the effect of gravity. At $t = 0.1$ s, the leading edge of water is slightly away from the obstacle. The experimental data show that a thin layer of liquid reaches the lower part of the obstacle. The wetness of downstream walls may affect the water acceleration. The obstacle is completely touched by the water at $t = 0.2$ s. A water tongue is created by the impact of water column to the obstacle. The agreement between experimental and numerical results is very good.

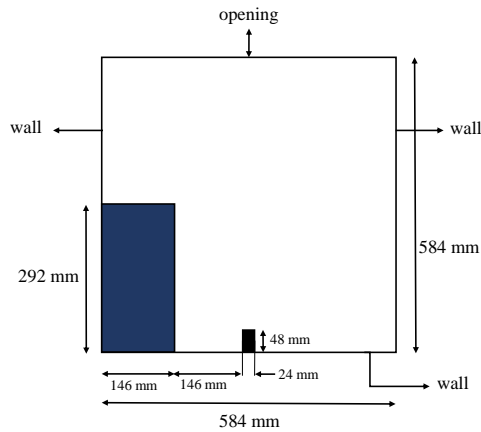


Fig. 9. Computational domain and boundary conditions for the dam break (TC3).

It can be seen that the small-scale air appears on the air water interface especially near the water tongue. At $t = 0.3$ s, by moving the water tongue toward the opposite wall, a part of tongue is separated and small water droplets are formed. The created water droplets are greater than the filter size and could be resolved by the numerical method. The dispersed small-scale air forms on the interface. After 0.4 s, the water tongue impacts to the opposite wall and entraps the air. The high level of turbulence created by the water impingement, increases the breakup process and consequently, the small air volume fraction rises. Due to the gravity effect, the water sheet starts to move downward at $t = 0.5$ s. A new water tongue is created near the obstacle and moves toward the opposite wall. At $t = 0.6$ s, the second water tongue impinges to the bottom wall and small air traps in the vicinity of the obstacle. A high level of dispersed air volume fraction is seen near the

water tongue impingement. The overall agreement between the results of multi-fluid numerical model and experimental data is well. The predicted distributions of large and small scales air agree well with experimental data.

The computed water height on the left wall is compared with the experimental data (Koshizuka 1995) and shown in Fig. 11. The experimental data are extracted via a picture digitizing process from the photos presented by Koshizuka (1995). The numerical results are in good agreement with both the experimental data (Koshizuka 1995) and the previous numerical VOF simulations (Issakhov *et al.* 2018). The maximum error of numerical simulations is less than 5%.

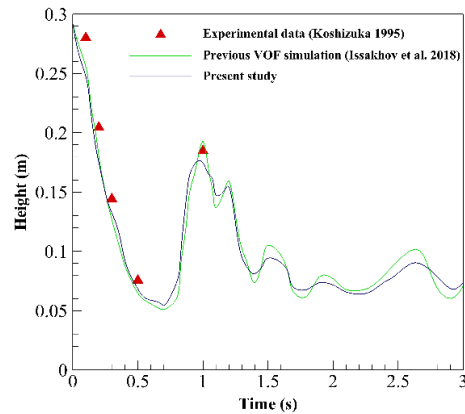


Fig. 11. Free surface height on the left wall of the domain compared to the experimental data (Ubbink 1997; Koshizuka 1995) and previous VOF results (Issakhov *et al.* 2018).

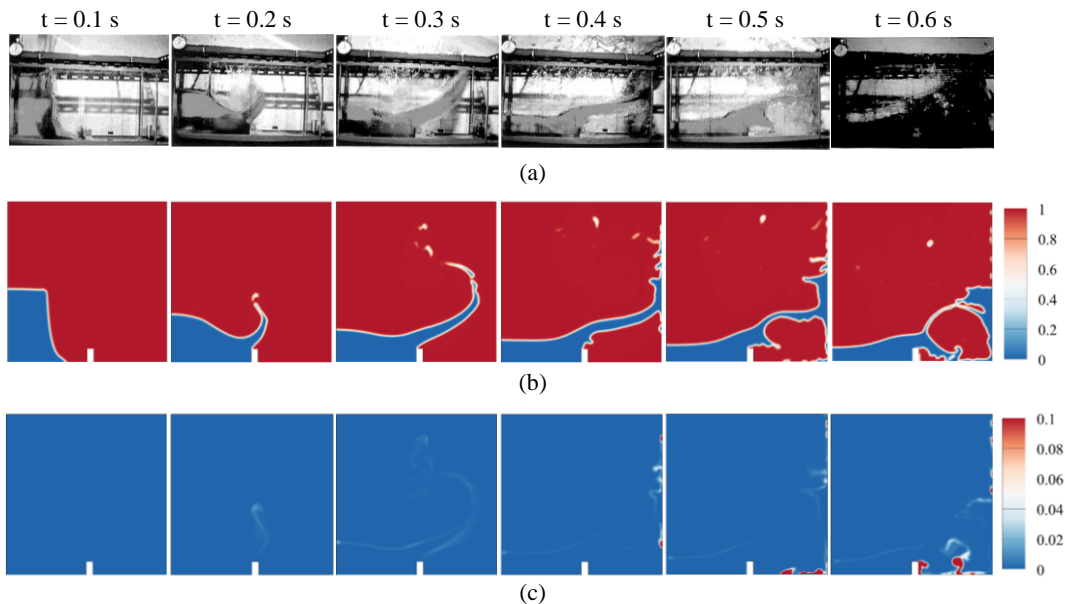


Fig. 10. Comparison experimental and numerical results of the dam break with obstacle, (a) experimental data (Koshizuka 1995; Ubbink 1997), (b) large-scale air, (c) small-scale air.

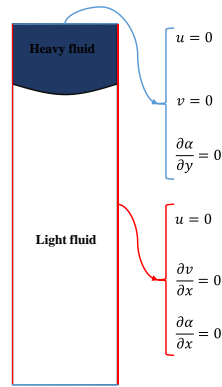


Fig. 12. Schematic of the computational domain and the boundary conditions for TC4.

4.4 Rayleigh Taylor Instability

The Rayleigh Taylor instability occurs in a system of two fluids with different densities in the existence of the gravity field. The heavy fluid is located over the light fluid. Due to the gravity effect, the heavy fluid moves underneath the light fluid. During the movement, the heavy fluid experiences the transition from stratified flow regime to the dispersed one and vice versa. Therefore, the Rayleigh Taylor instability is selected as TC4. The Rayleigh-Taylor instability problem was also used to validate the hybrid or two-fluid models (Cerne *et al.* 2001; Štrubelj and Tiselj 2008; Štrubelj and Tiselj 2011a,b). The simulations are performed in a 2D rectangle domain which contains two immiscible fluids with different physical properties. A heavy fluid with $\rho = 3 \text{ kg/m}^3$,

$\mu = 0.03 \text{ Pa}\cdot\text{s}$ and a light fluid with $\rho=1 \text{ kg/m}^3$, $\mu = 0.01 \text{ Pa}\cdot\text{s}$ are considered. The fluids are assumed to be isothermal and incompressible. The domain is discretized with the quadrilateral structured grid system. At the beginning of the simulation, the heavy fluid is set above the light fluid with the interface shape like a small cosine wave. The interface disturbance is shown in Eq. (6).

$$\delta = \delta_0 \left(\cos\left(\frac{2\pi x}{W} \pi - \pi\right) + 1 \right) \quad (6)$$

The width and height of the column are $W = 1 \text{ m}$ and $H = 5 \text{ m}$, respectively. The initial disturbance is set to $\delta_0 = 0.01 \text{ m}$ and the gravity is assumed to be $g = -9.8 \text{ m/s}^2$. The volume fraction of heavy fluid is 0.1. The no-slip boundary condition is considered on the top and bottom walls and the free slip boundary condition is utilized on the right and the left boundaries. A schematic of domain boundary conditions is shown in Fig. 12.

The present model, as a hybrid model, should be able to handle the transient multiscale multiphase flows. Figure 13 shows the simulation results of a complete dispersion and accumulation process of the heavy fluid. At the primary steps of the heavy fluid movement, the interfacial scale resolving approach is used. By increasing the velocity and instabilities on the interface, the breakup process starts, and the mass transfer from the large-scale to the small-scale heavy fluid occurs in the domain. As the flow regime changes to the dispersed flow, the interfacial scale averaging closure models is applied. Due to the induced vortices, the small-scale structures disperse all over the flow field. At the final stage, the heavy

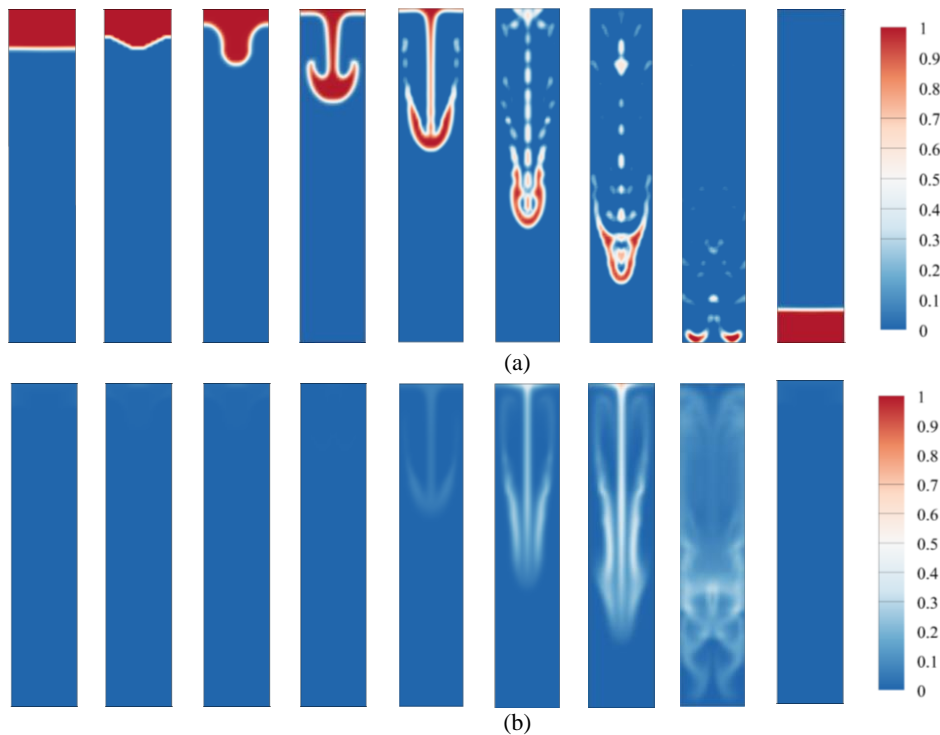


Fig. 13. Time variation of heavy fluid volume fraction, (a) large-scale heavy fluid, (b) small-scale heavy fluid.

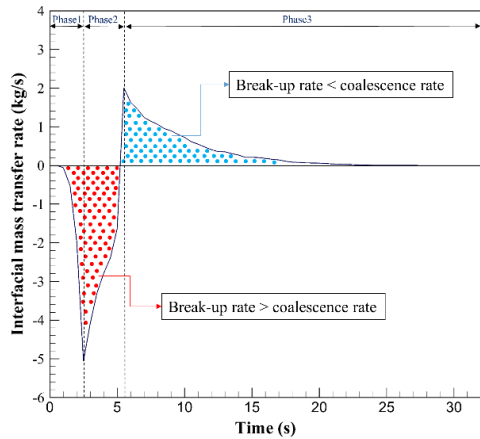


Fig. 14. Mass transfer rate over time between the large and small-scales air in TC4.

fluid settle on the bottom of cavity. The heavy fluid settling leads to the reverse transition and the small-scale particles aggregate together and the flow regime change from the dispersed to the segregated regimes.

Figure 14 shows the logged mass transfer rate between small and large scales over time. As the break-up process of large-scale structure begins, the mass transfer rate increases (Phase1). The negative sign for mass transfer rate represents that the break-up phenomenon prevails the coalescence phenomenon. As the large-scale structures reach the bottom of the column, the breakup rate is reduced and the mass transfer due to the coalescence phenomenon is dominated (Phase2). Over the time the mass transfer rate gradually decreases until all small-scale heavy fluid transferred to the large-scale heavy fluid (Phase3). Due to the mass conservation, the red dotted and the blue dotted areas are equal. The morphology transition from segregated flow to dispersed flow and vice versa is successfully captured by the present model. The obtained results prove the model's ability to solve a transient and multiscale problem. The developed solver has the capability of distinguishing between flow morphologies and choosing the appropriate approach between averaging and resolving the interface.

5. CONCLUSION

A multiscale Eulerian based solver in the context of OpenFOAM was developed in the present work. The transition between different morphologies was handled by adopting different closure modeling approaches. An LES-like approach was employed to distinguish between different morphologies. In the developed approach, the averaging length scale was utilized as a filter to adopt the appropriate closure models according to the underlying flow physics. The size groups characteristics were set according to the grid size in a way that the mass transfer between the phases occurs based on the averaging length scale. Therefore, the closure modeling framework was switched along with the coalescence or breakup

phenomenon. Four benchmark test cases were considered to assess the model's abilities and features. The mass transfer mechanisms from the small-scale to the large-scale phases and vice versa were evaluated by the bubble column and impinging jet benchmarks. The results showed the good agreement with the previous experimental data. The dam break benchmark with an obstacle was also investigated to show the model's capability to sharpen the interface between two large-scale phases. The results of Rayleigh-Taylor instability benchmark's also revealed the developed model's capability to successfully regenerate the physics of the transitional multiphase flows. The variations of the mass transfer rate between large and small scales demonstrated the models applicability for transitional multiphase flows.

The main conclusions are as follows:

- An LES-like approach based on structures equivalent diameter and averaging length scale was presented to identify the large-scale structures which makes the model independent to the unphysical regime recognition methods.
- Four different benchmark test cases were utilized to assess modelling approach. It is demonstrated that the model can reproduce the physical behaviour of different flow regimes including segregated, dispersed and complex flow regimes.
- The presented approach was a forward step to develop more physical and generalized models for multiscale multiphase flow simulations.

The turbulence multiphase flow and the effects of turbulence on the interfacial interactions, laminar-turbulent transition are still intact fields and considered for future researches.

REFERENCES

- Brackbill, J. U., D. B. Kothe and C. Zemach (1992). A continuum method for modeling surface tension. *Journal of computational physics* 100(2), 335-354.
- Brennen, C. E. (2005). *Fundamentals of multiphase flow*.
- Burns, A. D., T. Frank, I. Hamill and J. M. Shi (2004). May. The Favre averaged drag model for turbulent dispersion in Eulerian multi-phase flows. In *5th international conference on multiphase flow, ICMF* (Vol. 4, pp. 1-17). ICMF.
- Cerne, G., S. Petelin and I. Tiselj (2001). Coupling of the interface tracking and the two-fluid models for the simulation of incompressible two-phase flow. *Journal of computational physics* 171(2), 776-804.
- Chandrasekhar, S. (2013). *Hydrodynamic and hydromagnetic stability*. Courier Corporation.
- Cheung, S. C., G. H. Yeoh and J. Y. Tu (2007). On

- the numerical study of isothermal vertical bubbly flow using two population balance approaches. *Chemical Engineering Science* 62(17), 4659-4674.
- Coste, P. (2013). A large interface model for two-phase CFD. *Nuclear Engineering and Design* 255, 38-50.
- Danciu, D. V., F. Z. Kendil, A. Mishra, M. Schmidtke, D. Lucas and U. Hampel (2010). Velocity fields under impinging jets with gas entrainment. In *Proc. 7th Int. Conf. Multiphase Flow*.
- Denèfle, R., S. Mimouni, J. P. Caltagirone and S. Vincent (2015). Multifield hybrid approach for two-phase flow modeling—Part 1: Adiabatic flows. *Computers & Fluids* 113, 106-111.
- Gada, V. H., M. P. Tandon, J. Elias, R. Vikulov and S. Lo (2017). A large scale interface multi-fluid model for simulating multiphase flows. *Applied Mathematical Modelling* 44, 189-204.
- Greenshields, C. J. (2019). The OpenFOAM foundation user guide 7.0. *The OpenFOAM Foundation Ltd: London, United Kingdom, 10th July*.
- Hänsch, S., D. Lucas, E. Krepper and D. V. Danciu (2011). CFD-simulations of an impinging jet using a polydispersed multi-field model approach. *Transport Phenomena with Moving Boundaries* 6.
- Hänsch, S., D. Lucas, E. Krepper and T. Höhne (2012). A multi-field two-fluid concept for transitions between different scales of interfacial structures. *International Journal of Multiphase Flow* 47, 171-182.
- Höhne, T. and C. Vallée (2010). Experiments and numerical simulations of horizontal two-phase flow regimes using an interfacial area density model. *The Journal of Computational Multiphase Flows* 2(3), 131-143.
- Höhne, T., E. Krepper, D. Lucas and G. Montoya (2019). A multiscale approach simulating boiling in a heated pipe including flow pattern transition. *Nuclear Technology* 205(1-2), 48-56.
- Höhne, T., E. Krepper, G. Montoya and D. Lucas (2017). CFD-simulation of boiling in a heated pipe including flow pattern transitions using the GENTOP concept. *Nuclear Engineering and Design* 322, 165-176.
- Ishii, M. and N. Zuber (1979). Drag coefficient and relative velocity in bubbly, droplet or particulate flows. *AIChE journal* 25(5), 843-855.
- Issakhov, A., Y. Zhandaulet and A. Nogaeva (2018). Numerical simulation of dam break flow for various forms of the obstacle by VOF method. *International Journal of Multiphase Flow* 109, 191-206.
- Kolev, N. I. (2005). *Multiphase flow dynamics: Fundamentals*. Berlin, Germany: Springer.
- Koshizuka, S. (1995). A particle method for incompressible viscous flow with fluid fragmentation. *Comput. Fluid Dyn. J.* 4, 29.
- Krepper, E., D. Lucas, T. Frank, H. M. Prasser and P. J. Zwart (2008). The inhomogeneous MUSIG model for the simulation of polydispersed flows. *Nuclear Engineering and Design* 238(7), 1690-1702.
- Liao, Y., K. Upadhyay and F. Schlegel (2020). Eulerian-Eulerian two-fluid model for laminar bubbly pipe flows: Validation of the baseline model. *Computers & Fluids* 202, p.104496.
- Luo, H. (1995). Coalescence, breakup and liquid circulation in bubble column reactors.
- Luo, H. and H. F. Svendsen (1996). Theoretical model for drop and bubble breakup in turbulent dispersions. *AIChE Journal* 42(5), 1225-1233.
- Marschall, H. (2011). *Towards the numerical simulation of multi-scale two-phase flows* (Doctoral dissertation, Technische Universität München).
- Marschall, H. and O. Hinrichsen (2013). Numerical simulation of multi-scale two-phase flows using a Hybrid Interface-Resolving Two-Fluid Model (HIRES-TFM). *Journal of Chemical Engineering of Japan* 46(8), 517-523
- Mathur, A., D. Dovizio, E. M. A. Frederix and E. M. J. Komen (2019). A Hybrid Dispersed-Large Interface Solver for multi-scale two-phase flow modelling. *Nuclear Engineering and Design* 344, 69-82.
- Meller, R., F. Schlegel and D. Lucas (2021). Basic verification of a numerical framework applied to a morphology adaptive multifield two-fluid model considering bubble motions. *International Journal for Numerical Methods in Fluids* 93(3), 748-773.
- Melzer, D. I. D. (2018). Experimental Investigations on Impinging Liquid Jets with Gas Entrainment.
- Menter, F. R. (1994). Two-equation eddy-viscosity turbulence models for engineering applications. *AIAA Journal* 32(8), 1598-1605.
- Montoya, G., E. Baglietto and D. Lucas (2015). Implementation and validation of a surface tension model for the multi-scale approach GENTOP. In *Proceedings of the 16th International Topical Meeting on Nuclear Reactor Thermalhydraulics (NURETH-16)*. Chicago, USA.
- Montoya, G., E. Baglietto, D. Lucas, E. Krepper and T. Hoehne (2014, July). Comparative Analysis of High Void Fraction Regimes Using an Averaging Euler-Euler Multi-Fluid Approach and a Generalized Two-Phase Flow (GENTOP) Concept. In *International Conference on Nuclear Engineering* (Vol. 45950, p. V005T17A056). American Society of Mechanical Engineers.

- Parekh, J. and R. Rzehak (2018). Euler–Euler multiphase CFD-simulation with full Reynolds stress model and anisotropic bubble-induced turbulence. *International Journal of Multiphase Flow* 99, 231-245.
- Qu, X., L. Khezzar, D. Danciu, M. Labois and D. Lakehal (2011). Characterization of plunging liquid jets: A combined experimental and numerical investigation. *International Journal of Multiphase Flow* 37, 722-731.
- Rusche, H. (2002). Computational fluid dynamics of dispersed two-phase flows at high phase fractions. University of London.
- Schwarzkopf, J. D., M. Sommerfeld, C. T. Crowe and Y. Tsuji (2011). Multiphase flows with droplets and particles. *CRC press*.
- Shonibare, O.Y. and K. E. Wardle (2015). Numerical investigation of vertical plunging jet using a hybrid multifluid–VOF multiphase CFD solver. *International Journal of Chemical Engineering*.
- Shu, S., D. Vidal, F. Bertrand and J. Chaouki (2019). Multiscale multiphase phenomena in bubble column reactors: A review. *Renewable Energy* 141, 613-631.
- Štrubelj, L. and I. Tiselj (2008). Numerical Simulation of Rayleigh-Taylor Instability With Two-Fluid Model and Interface Sharpening. In *Fluids Engineering Division Summer Meeting* (48401), 33-42.
- Štrubelj, L. and I. Tiselj (2011a). Numerical simulations of basic interfacial instabilities with incompressible two-fluid model. *Nuclear Engineering and Design* 241(4), 1018-1023.
- Štrubelj, L. and I. Tiselj (2011b). Two- fluid model with interface sharpening. *International journal for Numerical Methods in Engineering* 85(5), 575-590.
- Tomiyama, A., H. Tamai, I. Zun and S. Hosokawa (2002). Transverse migration of single bubbles in simple shear flows. *Chemical Engineering Science* 57, 1849-1858.
- Tomiyama, A., I. Kataoka, I. Zun and T. Sakaguchi (1998). Drag coefficients of single bubbles under normal and micro gravity conditions. *JSME International Journal Series B Fluids and Thermal Engineering* 41, 472-479.
- Ubbink, O. (1997). Numerical prediction of two fluid systems with sharp interfaces.
- Van Leer, B. (1979). Towards the ultimate conservative difference scheme. V. A second-order sequel to Godunov's method. *Journal of computational Physics* 32, 101-136.
- Wardle, K. E. and H. G. Weller (2013). Hybrid multiphase CFD solver for coupled dispersed/segregated flows in liquid-liquid extraction. *International Journal of Chemical Engineering*.
- Weller, H. G. (2008). A new approach to VOF-based interface capturing methods for incompressible and compressible flow. OpenCFD Ltd., Report TR/HGW 4.
- Yan, K. and D. Che (2010). A coupled model for simulation of the gas–liquid two-phase flow with complex flow patterns. *International Journal of Multiphase Flow* 36(4), 333-348.
- Yeoh, G. H. and J. Tu (2009). Computational techniques for multiphase flows. *Elsevier*.
- Zhu, Y., H. N. Oğuz and A. Prosperetti (2000). On the mechanism of air entrainment by liquid jets at a free surface. *Journal of Fluid Mechanics* 404, 151-177.